buildings

MDPI

Article

Towards Greener 3D Printing: A Performance Evaluation of Silica Fume-Modified Low-Carbon Concrete

James Bradshaw [1], Swathi Balasubramanian [1,2], Wen Si [1,2], Mehran Khan [1,2,*] and Ciaran McNally [1,2,*]

[1] Centre for Critical Infrastructure, School of Civil Engineering, University College Dublin, D04 V1W8 Belfield, Ireland; swathi.balasubramanian@ucd.ie (S.B.); wen.si@ucd.ie (W.S.)
[2] Construct Innovate, School of Civil Engineering, University College Dublin, D04 V1W8 Belfield, Ireland
* Correspondence: khan.mehran@ucd.ie (M.K.); ciaran.mcnally@ucd.ie (C.M.)

Abstract

This study investigates the durability challenges of 3D-printed concrete (3DPC) and examines the effect of silica fume (SF) on its performance, focusing on mechanical properties and selected durability tests as key indicators of mix suitability for 3D printing applications. Five low-carbon mixes were prepared with 50% GGBS replacement and varying silica fume contents (2.5–10%), and were evaluated through slump, compressive strength, rapid chloride migration, and accelerated carbonation tests. The addition of GGBS reduced the concrete's shape retention, but incorporating silica fume improved flow behaviour, resulting in a more stable mix. The inclusion of GGBS and silica fume initially reduced 1-day strength but led to significant gains by 28 days, with the 5% SF low-carbon mix achieving the highest compressive strength. The low-carbon mixes showed superior chloride resistance, further enhanced by silica fume, though their carbonation resistance decreased with GGBS and SF addition. Overall, the 5% SF low-carbon mix demonstrated the best balance of strength, chloride resistance, and carbon reduction, despite minor trade-offs in early strength and carbonation resistance.

Keywords: 3D-printed concrete; silica fume; GGBS; low-carbon binders; durability performance; embodied carbon

check for updates

Received: 15 September 2025
Revised: 13 October 2025
Accepted: 18 October 2025
Published: 30 October 2025

Citation: Bradshaw, J.; Balasubramanian, S.; Si, W.; Khan, M.; McNally, C. Towards Greener 3D Printing: A Performance Evaluation of Silica Fume-Modified Low-Carbon Concrete. *Buildings* **2025**, *15*, 3919. https://doi.org/10.3390/buildings15213919

Copyright: © 2025 by the authors. Licensee MDPI, Basel, Switzerland. This article is an open access article distributed under the terms and conditions of the Creative Commons Attribution (CC BY) license (https://creativecommons.org/licenses/by/4.0/).

1. Introduction

Concrete structures are vulnerable to various forms of degradation, including corrosion, cracking, spalling, and damage from environmental exposures such as freeze–thaw cycles, carbonation, and chloride penetration [1]. Three-dimensional-printed concrete (3DPC) may be more susceptible to these conditions because in 3D printing, concrete is deposited in successive layers to build the desired form, enabling the constructional process to complete the structure [2]. However, this method may compromise durability compared to conventional construction techniques, as the interfaces between layers are more prone to deterioration from environmental exposure [3,4]. Developing a more durable concrete mix can help mitigate this issue, improving the performance of the structures in aggressive environments [5]. Enhanced durability also reduces the frequency of repairs, leading to lower maintenance costs and contributing to the long-term safety of the structure [6].Developing a concrete mix that not only enhances durability and performs well during the printing process but also promotes sustainability through the use of low-carbon binders is important to balance all the experimental and environmental aspects [7]. This can be achieved by using industrial by-products and some admixtures. "The addition of admixtures can change the

properties (including flowability, buildability and viscosity) of 3DPC to some extent" [8]. Another property that can be influenced by admixtures is durability. This project will examine the durability performance of a low-carbon concrete with GGBS and using silica fume (SF) as an admixture to improve both printability and durability. Reducing the amount of clinker in cementitious systems through the use of GGBS and SF has shown promise in lowering the embodied carbon in the production of concrete. Recent studies have extensively examined the role of GGBS in improving the performance and sustainability of conventional concrete. Its incorporation refines the pore structure, enhances secondary C-S-H formation, and reduces permeability, thereby improving durability and lowering embodied carbon [7]. Some previous works have involved low-carbon binders [9–13], and while these benefits are well established in traditional concrete, limited research has explored the application of GGBS in 3D-printed systems. Extending its use to 3D printing offers potential for developing low-carbon binders with enhanced strength, durability, and printability [14–18]. When added in the right proportions to cement, these elements can enhance the durability of concrete in addition to its environmental advantages. Potential areas that could contribute to the durability criteria include freeze–thaw resistance, chloride penetration resistance, carbonation resistance, sulfate resistance, etc. When assessing the durability of concrete while changing its composition, it is common to examine the resistance to these processes [19]. An example of this is Zhou et al.'s 2024 study, "Durability and hardened properties of 3D-printed concrete containing bauxite tailings" [20]. It is also important to ensure that the mix still performs well in terms of printability; slump and rheology testing will help determine this prior to testing the mix in the printer [21,22].

It is known that 3DPC has significant potential to enhance sustainability in the construction industry. One of its key advantages is the precision it offers in material usage, and accurate digital modelling enables concrete to be placed exactly where it is needed, reducing overproduction and minimizing onsite waste. This efficiency not only cuts down raw material consumption but also lowers energy demands related to transport and formwork fabrication, as 3DPC eliminates the need for traditional moulds [23]. The environmental benefits can be further amplified by incorporating low-carbon concrete mixes. The importance of this research lies in the development of 3DPC, which is more viable and can have huge social, economic, and environmental benefits for the construction industry. Several parts of the world are experiencing a shortage of housing. Three-dimensional printing can offer a reduction in production time in the construction by 50% to 70%, which would help to construct more houses faster [24]. One Irish example of using 3D printing for housing is the social housing development at Grange Close in Dundalk, seen during construction in Figure 1 [25]. In terms of economic benefits, there is a 50% to 80% reduction in labour costs associated with 3D-printed construction when compared to traditional construction techniques [24,26]. Lastly, there is a possible 30% to 60% reduction in construction waste [24]. As a technique, 3DPC is precise and prevents excess concrete from being produced and going to waste; it also reduces waste related to the formwork used in traditional concrete construction methods. Moreover, 3DPC can also utilize low-carbon mixes with reduced cement content, compounding the reduction in carbon emissions [27,28]. Using these low-carbon binders in 3D printing concrete mixes is a potential innovative step in creating durable and environmentally friendly building materials.



Figure 1. A completed 3D-printed house in Grange Close, Dundalk [29].

Previous studies on 3DPC have predominantly concentrated on mixtures based on conventional Portland cement, with significant attention given to optimizing mix designs to ensure printability and mechanical performance [30–32]. There has been minimal research on incorporating low-carbon binders into 3DPC, especially with respect to analyzing their fresh and mechanical properties [33,34]. However, there is a noticeable research gap in the application of low-carbon binders in 3DPC, particularly concerning their long-term durability characteristics. Considering the shift toward environmentally responsible building practices, a comprehensive evaluation of the durability of 3DPC with sustainable binder alternatives is both relevant and necessary. This study addresses this gap by introducing a novel approach to 3D-printable concrete using low-carbon binders. Specifically, CEM II-based concrete was used as a reference mix, and its performance was compared with mixes in which 50% of the cement was replaced with GGBS. To further enhance the properties of the mix, SF was incorporated in varying dosages of 0%, 2.5%, 5%, 7.5%, and 10%. Traditional 3D concrete printing primarily relies on ordinary Portland cement as the main binder. In contrast, this study adopts low-carbon materials such as SF to develop a more sustainable matrix. Additionally, SF contributes to improved flow characteristics, which is essential for printing. These findings underscore the importance of incorporating SF in low-carbon 3D-printable binders to achieve both environmental benefits and printing performance. The water-to-binder ratio was maintained constant across all mixes, and the influence of SF on durability was assessed. This research primarily focuses on two critical durability parameters; these are resistance to chloride ion penetration, assessed through the Rapid Chloride Migration test, and carbonation resistance, evaluated using the Accelerated Carbonation Penetration Test. This integrated approach not only provides insights into the viability of low-carbon binders for the potential application of 3DPC but also contributes to advancing sustainable construction practices through innovative material solutions.

2. Methodology

2.1. Materials and Mix Composition

The different binders used for 3DPC were cement (CEM), ground granulated blast furnace slag (GGBS), and Silica Fume (SF). The CEM used was Irish Cement Type II Portland cement compliant with I.S. EN 191-1 [35]. The GGBS was provided by Ecocem, which was compliant with I.S. EN 15167-1 [36]. The SF was provided by Sika Ireland Ltd and was

compliant with I.S. EN 13263-2 [37]. The aggregate consisted of sand, crushed rock fine (CRF), and a coarse aggregate. Sand and CRF were provided by Roadstone. Limestone rock with a maximum particle size of 10 mm was used for the coarse aggregate, also provided by Roadstone. Sika ViscoCrete-10 from Sika Ireland Ltd was the liquid-based admixture used as a superplasticiser (SP) [38]. The coarse aggregate ratio (coarse aggregate/(coarse aggregate + CRF + sand)) was 0.4. After trial mixing, a water-to-binder ratio (w/b) of 0.45 was selected, and an SP dosage of 1% of the mass of the binder was added. Table 1 gives a summary of the mixes used for 3DPC. Two control mixes were used: C100 with a 100% cement binder and CG with a 50% cement, 50% GGBS binder. The test mixes had a binder of 50% GGBS and an SF content ranging from 2.5% to 10% as a replacement for cement. The structured methodology for assessing the properties of the low carbon concrete is as shown in Figure 2.

Table 1. Mix compositions.

	Unit	C100	CG	CGS2.5	CGS5	CGS7.5	CGS10
CEM	Kg/m^3	350	175	166.25	157.5	148.75	140
GGBS	Kg/m^3	0	175	175	175	175	175
SF	Kg/m^3	0	0	8.75	17.5	26.25	35
Water	Kg/m^3	157.5	157.5	157.5	157.5	157.5	157.5
Sand	Kg/m^3	850	850	850	850	850	850
CRF	Kg/m^3	283.3	283.3	283.3	283.3	283.3	283.3
C10	Kg/m^3	750	750	750	750	750	750
SP	Kg/m^3	3.5	3.5	3.5	3.5	3.5	3.5
W/B		0.45	0.45	0.45	0.45	0.45	0.45
SP/B		0.01	0.01	0.01	0.01	0.01	0.01

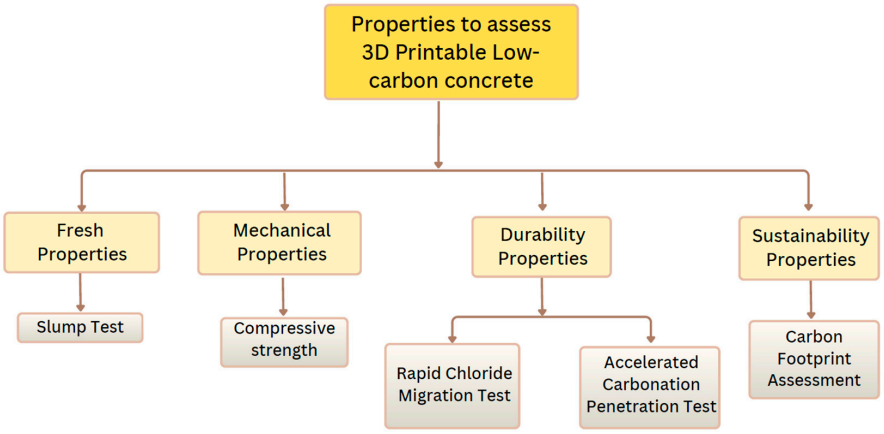


Figure 2. Methodology of this study.

Table 2 below contains the carbon factors (kg of CO_2/tonne) of each of the materials used for concrete mixes in this paper. The carbon factors of CEM, GGBS, SF, 10 mm aggregate and SP were obtained from the Environmental Product Declarations (EPDs) under the module cradle-to-gate (A1–A3). The carbon factor for the CRF and the sand was selected based on literature [39]. The carbon factor of water was deemed insignificant and was consistent across the mixes; thus, it was not included in the calculation. These factors were used to calculate the quantity of carbon dioxide emissions associated with one tonne of each of the mixes. All laboratory work was conducted under strict safety protocols.

Table 2. Carbon factor of each mix constituent.

Constituent	Cement	GGBS	SF	Sand	CRF	C10	SP
Carbon Factor ($kgCO_2$/tonne)	698 [40]	43 [41]	28 [42]	7.7 [39]	8.5 [39]	6.89 [43]	1260 [44]

2.2. Mixing

Mixing was carried out using the Concrete Mixer 56/40 Litre Capacity (forced action pan mixer), ELE International, Leighton Buzzard, UK. Firstly, the dry constituents were added in layers: coarse aggregate, CRF, sand, GGBS, CEM and then SF. The layered materials were dry-mixed for 60 s. Water and superplasticiser were premixed and gradually added to the mix. The wet mixing was carried out for 300 s based on optimal flow behaviour determined from trial batches. Then, the mixing was intermittently paused to remove adhered material from the blades, followed by a final 60 s mixing cycle.

2.3. Casting and Curing

It was found from the trial mixes that the mixes were flowable and did not require tamping or vibration during casting, as this could cause over-vibration or bleeding of the sample. Prior to casting, the moulds were coated with a layer of strike release oil. The 100 mm cube moulds were half-filled with concrete before being raised and dropped from 10 cm for self-compaction. The mould was then filled to the top, and excess concrete was removed. The same process for self-compaction was carried out to remove air voids from the concrete. Similarly, the 100 mm Ø × 50 mm disk moulds and 75 mm × 75 mm × 200 mm prisms were filled with concrete by the same procedure. However, due to the weight of the metal moulds, one side was lifted and dropped at a time for self-compaction before filling the moulds and repeating the process. Figure 3 shows the samples in the moulds directly after casting. Once the moulds were cast, they were covered to avoid loss of moisture. A small piece of plastic was used for each sample, then a layer of hessian cloth, and finally a large layer of plastic covering all samples. The samples were removed from the moulds approximately 16–24 h after casting in line with I.S. EN 12390-2 [45]. The cube samples were removed from the moulds using an air compressor, and the disks and prism moulds were disassembled. After the samples were removed from the moulds, they were placed in a water tank, as shown in Figure 4. They were kept at 20 ± 2 °C until the desired curing age, compliant with I.S. EN 12390-2 [45].



Figure 3. Cast samples.

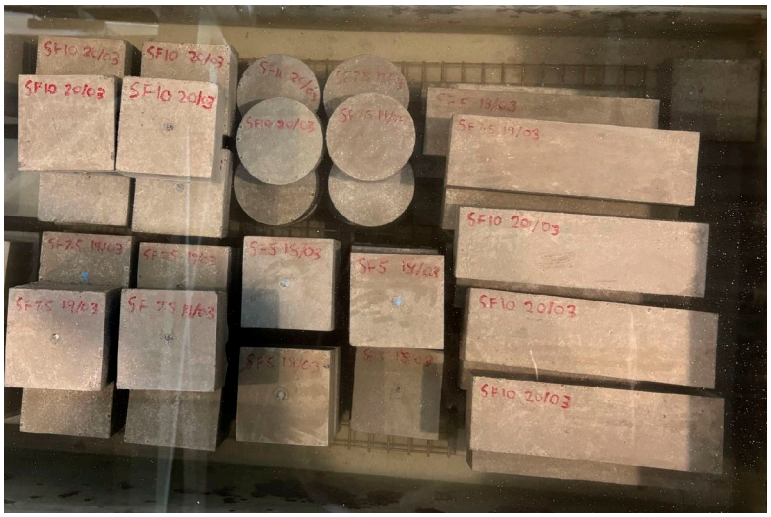


Figure 4. Samples curing in the water tank.

2.4. Testing Procedures

2.4.1. Slump Test

The slump test was conducted immediately upon completion of the mixing process. Prior to testing, the mould was wetted and placed on a flat surface. Concrete was filled into the top of a mould, and this was carried out within 2 min as recommended for high-flowability mixes in ISO 1920-2:2016 [46]. Due to the high flowability of the concrete, the cone was filled in one layer, and tamping was deemed unnecessary. The mould was then lifted vertically, and the slump height was recorded to the nearest 5 mm.

2.4.2. Compressive Strength Test

A total of nine cube samples were made for each mix. This allowed three samples to be tested in 1, 7 and 28 days. The Controls Automax5 50-C56V2 automatic compression tester, Controls Group, Milan, Italy was used. The samples were placed in a proper orientation for reliable results.

A constant loading rate of 0.6 ± 0.2 MPa/s was applied to the samples, as per I.S. EN 12390-3:2019 [47]. A satisfactory cube failure after testing is identified by the large vertical cracks at the corners of the sample. The average of the results from testing the three samples gives the compressive strength of the mix during each curing period.

2.4.3. Rapid Chloride Migration Test

The chloride migration test was carried out 28 ±1 days after the samples of each mix were cast with a 100 mm diameter and 50 mm height. The samples were left in the water bath until immediately before testing. The samples were fitted at the bottom of the rubber sleeves, and stainless steel clamps were fitted around the outside of the sleeve and tightened to the top and bottom of the samples to ensure the solution only had contact with the top and bottom of the sample. The anolyte solution consisted of 0.3 M NaOH solution, and the catholyte solution consisted of 5% NaCl solution. The catholyte solution was added to the catholyte reservoir, the plastic container. The anolyte solution was then added to the rubber sleeve until it reached a minimum of 10 mm above the sample.

An initial voltage of 30 V based on I.S. EN 12390-18 [48] was applied to the sample using a power supply. The test voltage and duration for each sample were determined based on the voltages and corresponding currents as per the guidelines given in I.S. EN 12390-18. Through this procedure, it was determined that 25 V would be applied to mix C100 for 24 h and that 30 V would be applied to all other mixes for 48 h.

Once the test was completed, the samples were removed from the apparatus, and they were split lengthwise while still wet. The split samples were placed with the chloride-exposed side facing down. The fractured surface was covered with silver nitrate solution. The silver nitrate solution was applied a second time after 10 min. The samples were then left for 30 min to allow the penetration depth to become more visible. Figure 5 shows how the penetration depth was measured at 9 points, excluding 10 mm in from each edge, as described in I.S. EN 12390-18:2021+A1:2024 [48].



Figure 5. Method for measuring chloride depth.

The average of the penetration depth from both halves of each sample was used as x_d in mm. Equation (1) below was used to calculate the migration coefficient, M_{nss}. T is the absolute temperature in K, h is the height of the sample in mm, U is the voltage applied to the sample in V, and t is the test duration of the sample in h.

$$M_{nss} = \frac{0.0239(T)h}{(U)t}\left(x_d - 0.0186\sqrt{\frac{(T)hx_d}{(U)}}\right) \quad (1)$$

2.4.4. Accelerated Carbonation Penetration Test

Two 75 mm × 75 mm × 250 mm prism samples were cured in water for 28 ± 1 days for each mix. A shortened preconditioning process based on GB T50082-2009 was carried out [49]. The samples were subjected to 2 days at 60 °C as opposed to the 14 days conditioning at 20 °C as per I.S. EN 12390-12:2020 [50]. The shortened pre-conditioning step can accelerate carbonation kinetics. As a result, the absolute carbonation depths measured in this study may not directly represent natural exposure conditions. An AUTOFLOW IR Water-Jacketed CO_2 Incubator was used as the carbonation chamber. Although the trays of the carbonation chamber were perforated, each sample was placed on top of Perspex spacers to allow unobstructed airflow to all faces of the sample, as shown in Figure 6. The trays were then placed in the carbonation chamber, as shown in Figure 7a.

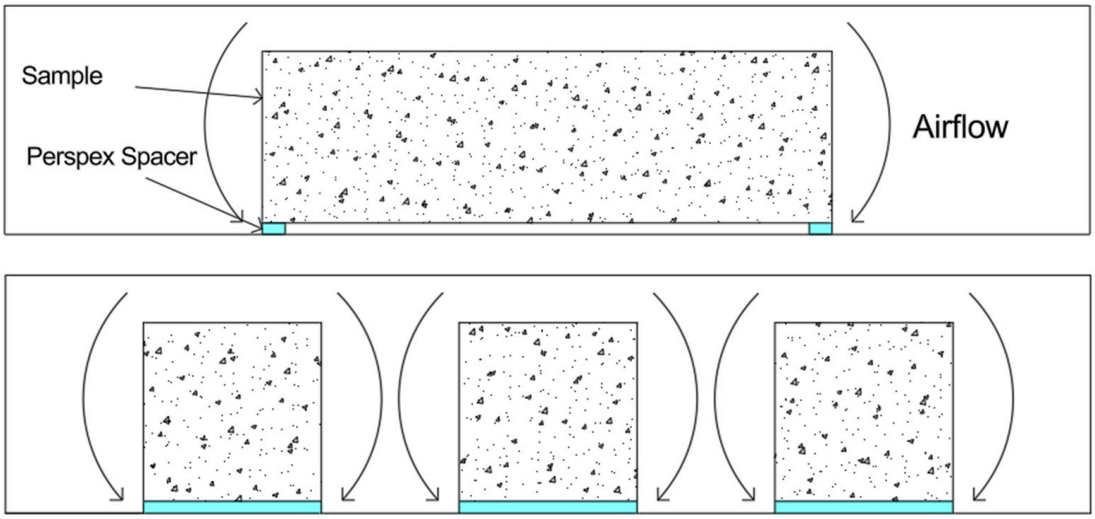
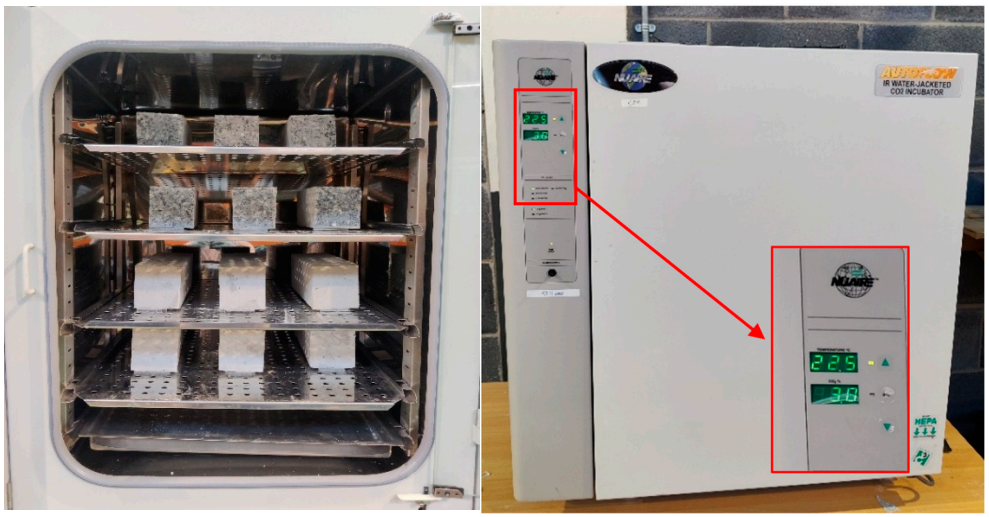


Figure 6. Layout of carbonation samples.



(**a**) (**b**)

Figure 7. (**a**) Samples in carbonation chamber and (**b**) controls in carbonation chamber.

Once all samples were in the carbonation chamber, the carbon dioxide concentration was increased to 3% using the controls shown in Figure 7b, as per I.S. EN 12390-12:2020 [50].

The samples were removed from the carbonation chamber at 7, 14, and 28 days. A 50 mm slice was split from the end of the sample of each sample at each exposure period, and the sample was returned to the carbonation chamber. A solution of 0.8 g of phenolphthalein dissolved in 70 mL of ethanol and 30% deionized water was made. It was applied to the split face of the sample. The carbonation depth was recorded at five points on each of the four faces in accordance with I.S. EN 12390-12:2020. The five points were selected by dividing the length of the face into four sections, as shown in Figure 8. The carbonation depth was measured at each point to the nearest 0.5 mm. The carbonation depth was taken as the average depth across the two samples. Equation (2) below shows the formula used to calculate d_k, the average carbon penetration depth. The average carbon penetration depths are graphed against exposure time in days t. The y-intercept is in mm, and the slope is the carbonation rate K_{AC} in mm/$\sqrt{}$days.

$$d_k = a + K_{AC}\sqrt{t} \quad (2)$$

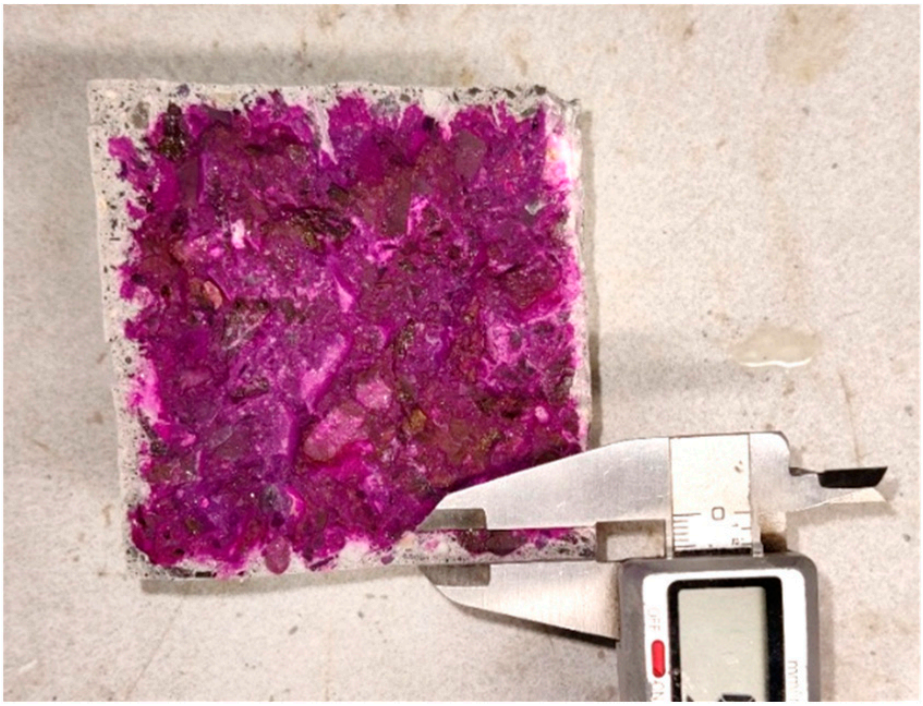


Figure 8. Method for measuring carbonation depth.

3. Results

3.1. Carbon Footprint Assessment

The carbon footprint of each concrete mix was calculated based on the embodied carbon values derived from Environmental Product Declarations (EPDs) as described in Section 3.1. Among the materials used, CEM exhibited the highest embodied carbon at 698 $kgCO_2e$/tonne, whereas GGBS had a considerably lower value of 42 $kgCO_2e$/tonne, and SF further reduced emissions at just 28 $kgCO_2e$/tonne. This substantial variation in carbon intensity plays a critical role in the overall environmental performance of the mix designs. The mixes that used 50% GGBS replacement have much lower carbon emissions, as CEM has more than 16 times the embodied carbon of GGBS. Table 3 below shows the embodied carbon of one tonne and one cubic metre, as well as the density of each of the concrete mixes used in this research. The reference mix C100, composed entirely of CEM, showed the highest carbon emissions at 285.9 $kgCO_2e/m^3$, as depicted in Figure 9. In contrast, the progressive incorporation of GGBS and SF led to a significant reduction in emissions. The CG mix, which includes 50% GGBS as a binder replacement, resulted in a notable 41% reduction, bringing emissions down to 168.0 $kgCO_2e/m^3$. Further enhancement was achieved through the partial replacement of GGBS with SF in the CGS series, where carbon emissions dropped incrementally from 161.8 $kgCO_2e/m^3$ in CGS2.5 to just 143.4 $kgCO_2e/m^3$ in CGS10.

Table 3. Embodied carbon of each mix.

Constituent	C100	CG	CGS2.5	CGS5	CGS7.5	CGS10
$kgCO_2e$ per tonne	109.772	61.899	59.450	57.002	54.553	52.105
$kgCO_2e$ per m^3	268.915	151.035	144.890	138.760	132.644	126.542
Density (kg/m^3)	2449.762	2440.042	2437.174	2434.313	2431.459	2428.611

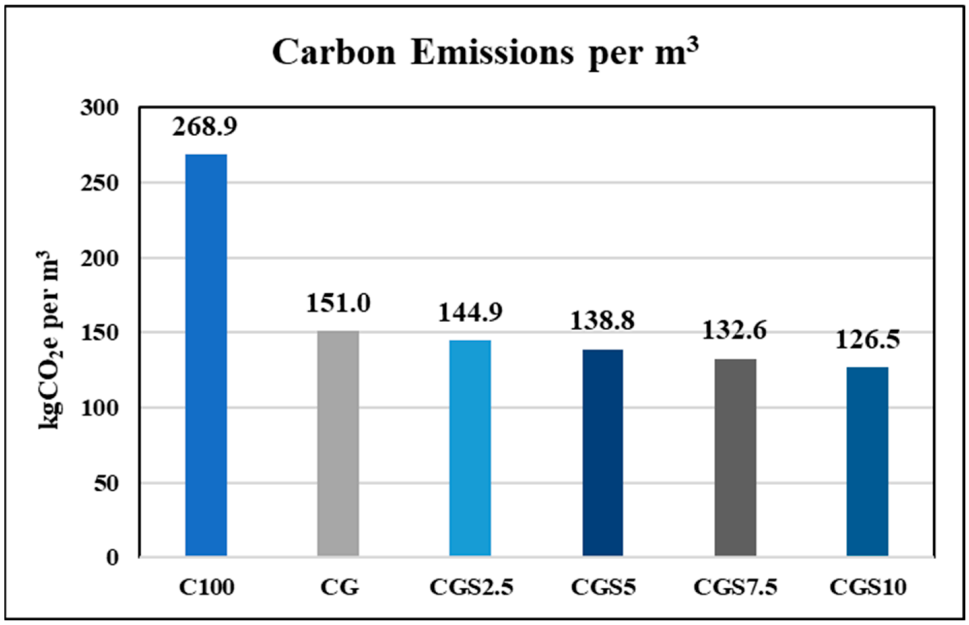


Figure 9. Carbon emissions per m^3 of concrete.

This steady decline underscores the effectiveness of using low-carbon binders in reducing the embodied carbon of concrete. The reductions are attributed not only to the inherently lower carbon intensity of GGBS and SF but also to the optimized synergy between these supplementary cementitious materials. The data reinforces the potential of these blended systems to meet sustainability targets without compromising performance, making them suitable for eco-friendly construction practices.

3.2. Slump Test

Figure 10 depicts the slump test performed on each mix, and the results are tabulated in Table 4. Mix CG had the greatest measured slump at 26.5 cm. The smallest measured slump was mix CGS10 at 19.5 cm. The control mix C100 and mix CGS7.5 behaved similarly in both measured slump and the shape retention upon removal of the slump cone. It is clear that using GGBS as a cement replacement greatly increases the flowability of the mix. This is due to the reduced water demand as GGBS particles allow better packing. The addition of GGBS improves the distribution of particles, which increases the fluidity and workability of the mix [51]. As the percentage of SF replacement is increased, the flowability decreases and the ability of the mix to retain its shape increases. This behaviour is attributed to the higher water demand required to adequately disperse the finer SF particles [52].

Table 4. Average measured slump for each mix.

Mix	C100	CG	CGS2.5	CGS5	CGS7.5	CGS10
Measured Slump (cm)	22.5	26.5	25.5	23.5	21	19.5

The influence of the GGBS and SF on the flowability of the mixes is represented in Figure 11. The increase in the measured slump between mix C100 and mix CG is due to the addition of GGBS. The addition of 2.5% SF decreases the measured slump. A similar reduction in flow due to the addition of silica fume was observed in a previous study on 3D-printed concrete [53]. As the quantity of SF continues to increase, the measured slump decreases linearly.

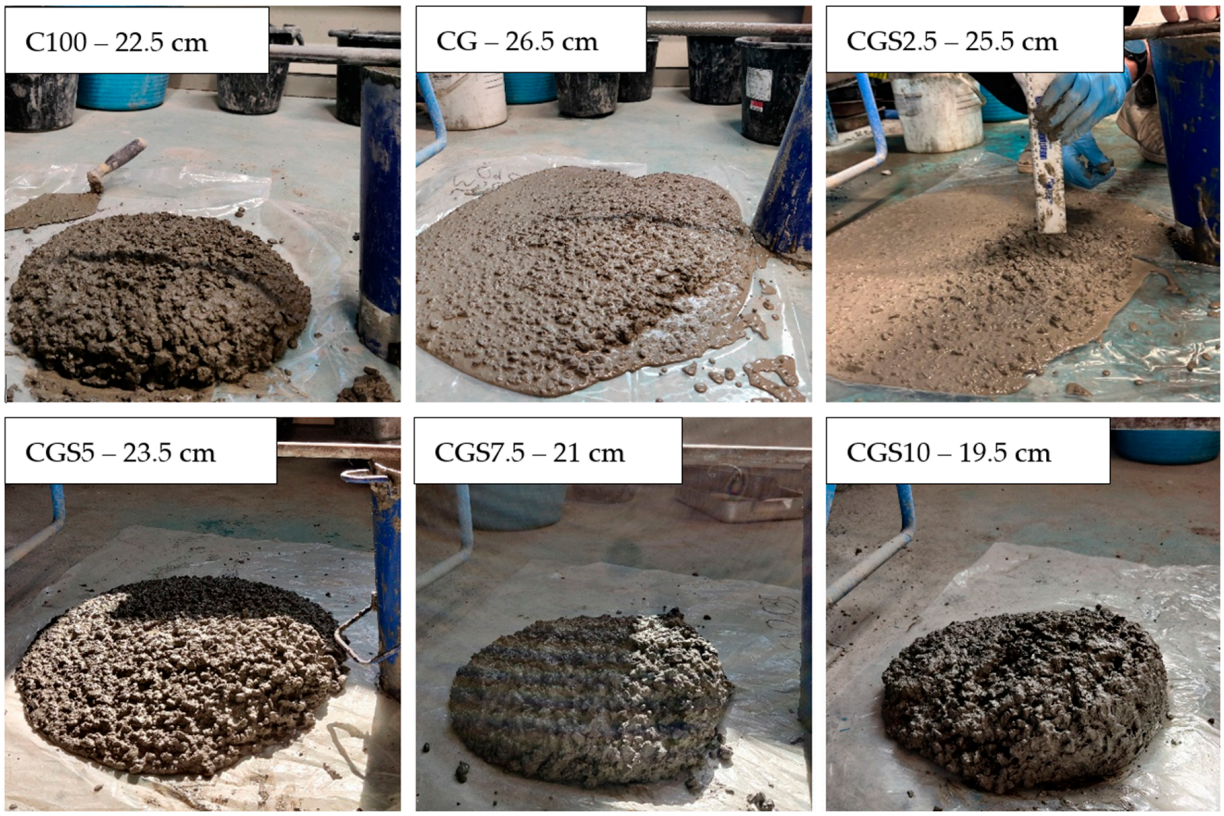


Figure 10. Slump of each mix.

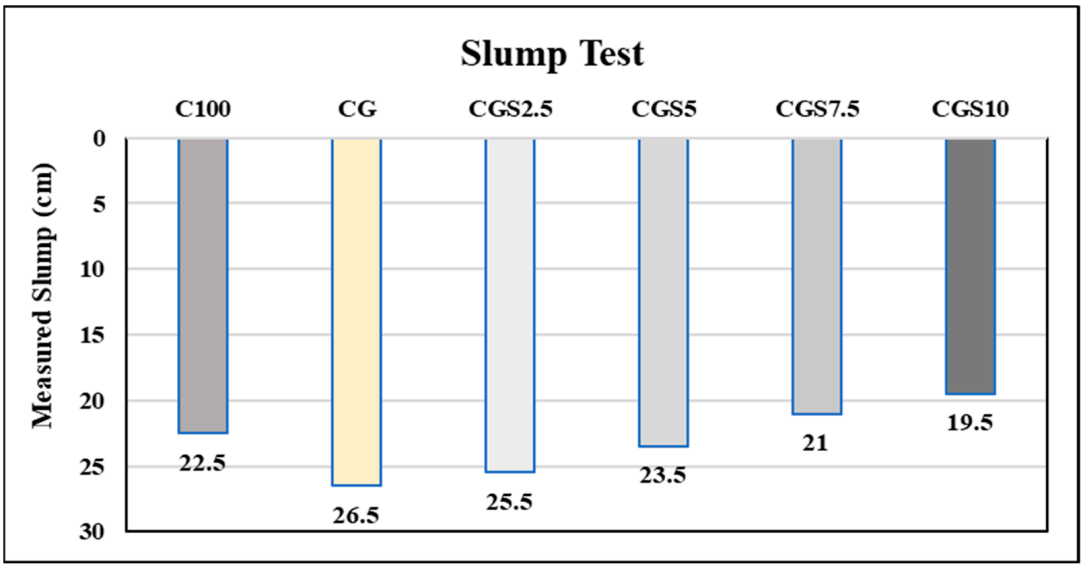


Figure 11. Slump flow results across mixes.

3.3. Compressive Strength

Figure 12 displays the impact of SF on the compressive strength results after 1-day curing. The results show that C100 has the highest early-age strength (1-day compressive strength) by a notable margin, with a strength of 36.1 MPa. The addition of GGBS in CG reduced the early-age strength to 15 MPa, which is a 58.5% reduction in strength. Among the ternary blends (CGS series), the inclusion of SF led to only marginal improvements or slight variations in early strength. CGS2.5 exhibited a peak of 15.7 MPa, slightly higher than CG, likely due to the filler effect. However, further increases in SF content resulted in

a decline, with CGS10 reaching only 14.1 MPa. The lowest strength among the CGS series was achieved in CGS7.5 with an early-age strength of 13.9 MPa.

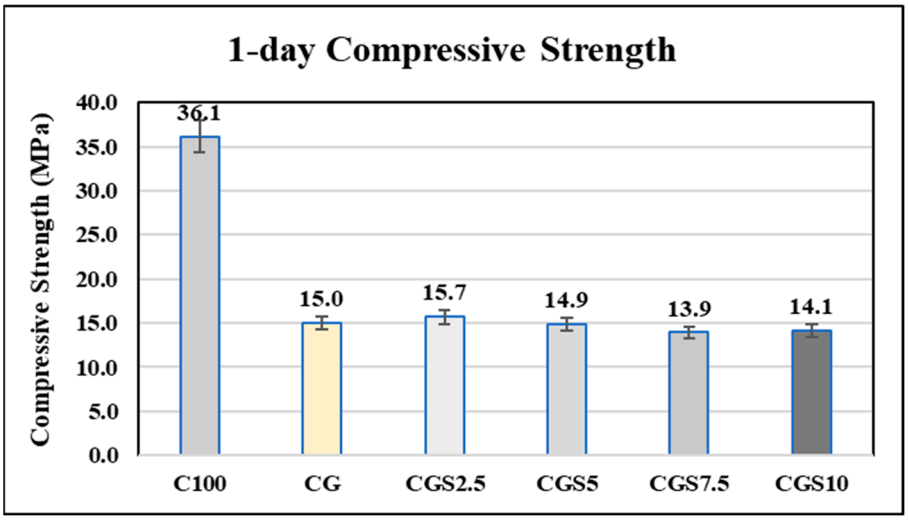


Figure 12. One-day compressive strength results across mixes.

Figure 13 compares the 7-day compressive strength and the effect of SF on this strength. Similarly to the 1-day compressive strength, C100 had the largest 7-day compressive strength at 48.8 MPa. Another similarity is the decrease in strength due to GGBS addition; however, the proportion of the decrease was greatly reduced. CG had a strength of 43 MPa at 7 days, a decrease of 12% in 7-day strength compared to C100. Among the CGS mixes, CGS5 recorded the lowest strength at 37.3 MPa, and the further inclusion of SF continued to cause a reduction in compressive strength.

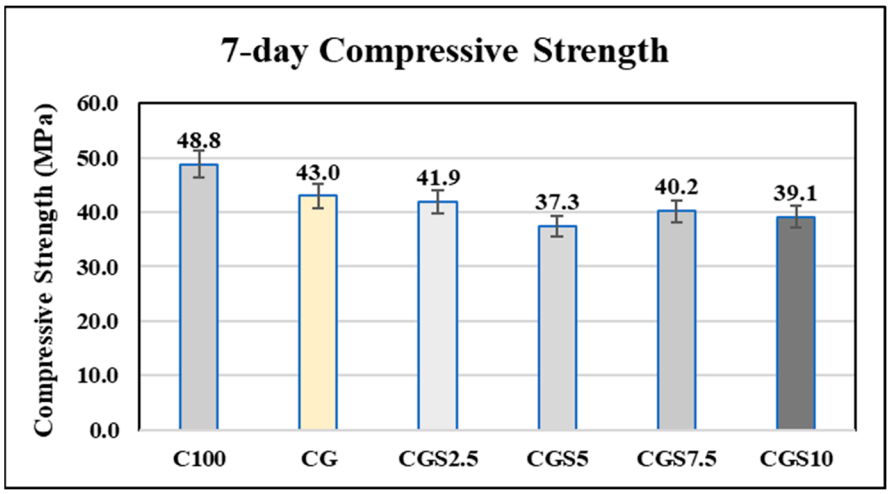


Figure 13. Seven-day compressive strength results across mixes.

Figure 14 displays the 28-day compressive strength results. The trend of the results changed significantly at 28 days compared to earlier curing periods. Unlike the 1-day and 7-day compressive strengths, the control mix C100 exhibited the lowest 28-day strength at 56.3 MPa. The addition of GGBS increased the strength moderately by 4.2% to 58.6 MPa. Further enhancement was observed with the addition of SF. CGS5 had the highest strength at 59.6 MPa, a 6% increase compared to C100. The compressive strength began to decrease when the SF content reached 7.5%, which suggests that the optimum SF content lies between 2.5% and 7.5%.

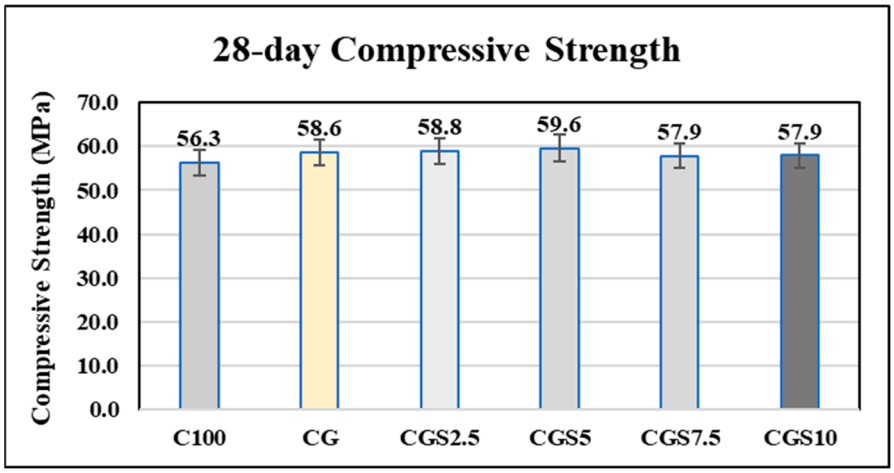


Figure 14. Results of 28-day compressive strength across mixes.

Figure 15 demonstrates the compressive strength trends of all mixes. The large difference between C100 and all the mixes containing GGBS is distinct in 1-day strength. At 7 days, the difference between C100 and GGBS (CG) mixes greatly diminished, and further reductions were observed in the CGS mix series. At 28 days, all modified mixes exhibited higher compressive strength than the control mix C100. Among them, CGS5 showed the highest strength, followed by CGS2.5 and CGS7.5, as illustrated in Figure 14.

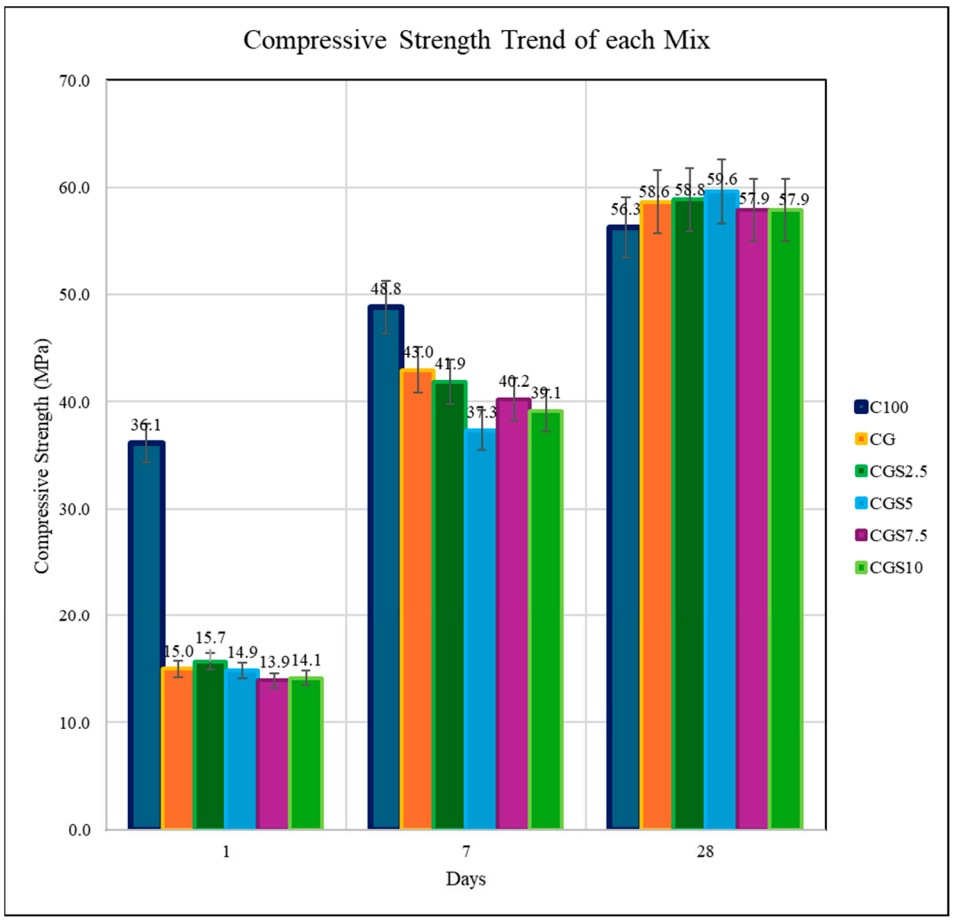


Figure 15. Plot of compressive strength trends.

3.4. Rapid Chloride Migration

Figure 16 shows the chloride penetration depth that was measured after the samples were split and sprayed with 0.1 N silver nitrate solution. The penetration depths were recorded at the edge of the silver area outlined in red. C100 had a chloride penetration depth of 30.1 mm after experiencing 25 V for 24 h. The rest of the mixes experienced 30 V for 48 h and had a chloride penetration depth of 15.7, 14.7, 11.2, 9.8, and 8.9 mm for mixes CG, CGS2.5, CGS5, CGS7.5, and CGS10, respectively.

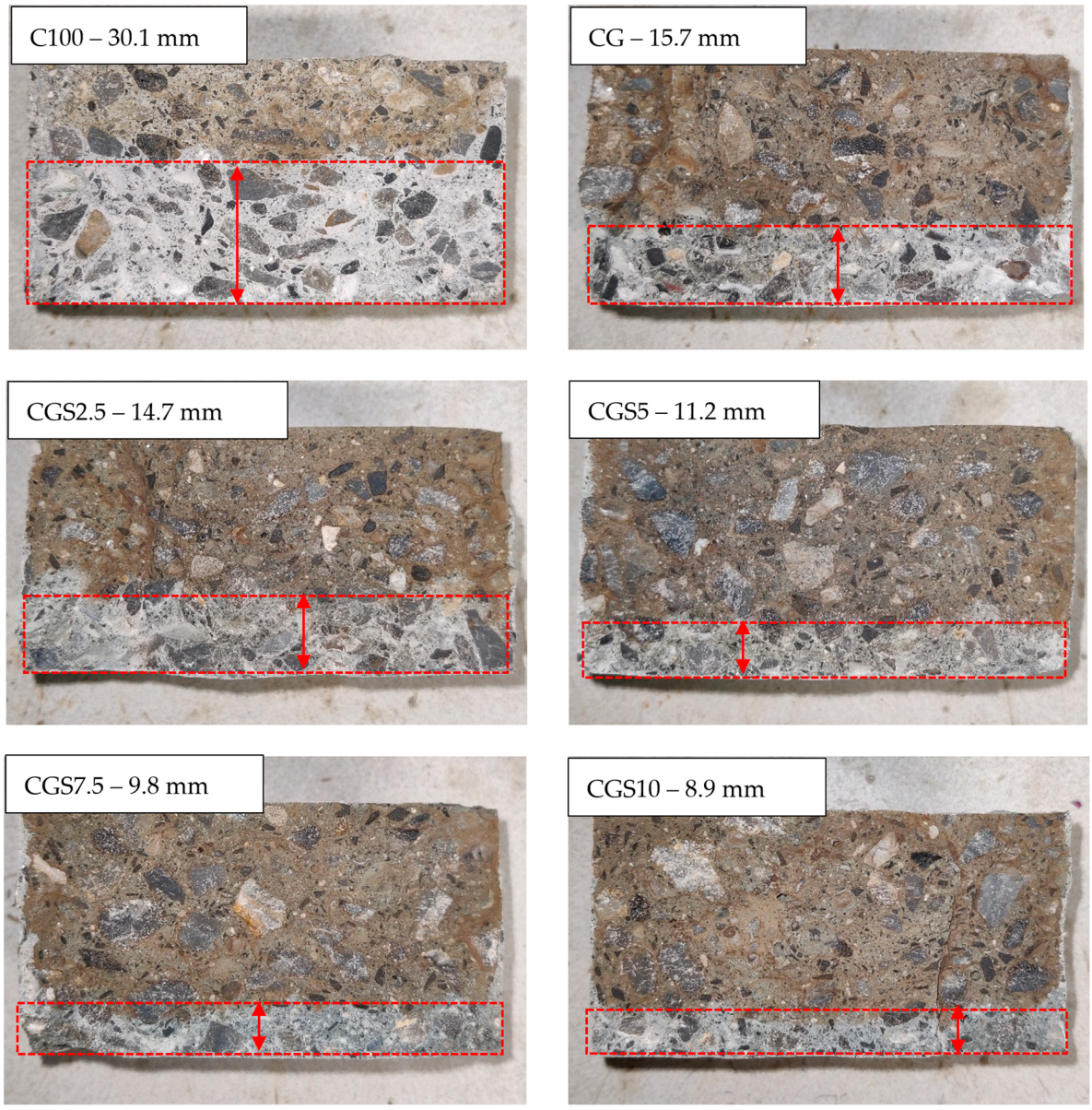


Figure 16. Chloride penetration depth in samples.

Figure 17 compares the chloride migration coefficient of all mixes. The control mix, C100, exhibited the highest migration coefficient at 16.1 × 10^{12} m^2/s. The inclusion of GGBS in the CG mix significantly reduced this value, improving chloride resistance by a factor of 4.7, with a migration coefficient of 3.422 × 10^{12} m^2/s. This enhancement is likely attributed to the denser microstructure associated with concrete containing GGBS, which refines the pore structure through the formation of calcium silicate hydrate (C-S-H) gel during hydration [31]. Additionally, the high aluminate content in GGBS contributes to chloride binding by forming Friedel's salts, thereby limiting chloride ion mobility [31].

The incorporation of SF further improved chloride resistance, though the effect was less pronounced compared to the addition of GGBS. The CGS10 mix demonstrated the lowest chloride migration coefficient at 1.872 × 10^{12} m^2/s, making it 8.6 times and 1.8 times more resistant to chloride ingress compared to C100 and CG, respectively. The superior performance of CGS10 relative to the control mix highlights the beneficial effect of incorporating SF into the CG mix. The synergistic effect of cement, GGBS, and SF in the ternary blend can be attributed to their complementary particle size distribution. GGBS particles, being relatively finer than cement but coarser than SF, help fill the intermediate voids, while the SF occupies the micro-pores between GGBS and cement grains. This multi-scale packing leads to a more continuous and dense particle arrangement, reducing porosity and enhancing the solid volume fraction of the paste. Consequently, the concrete exhibits higher compressive strength and reduced permeability, reflecting the beneficial influence of optimized particle packing in the ternary system [51]. Furthermore, the pozzolanic reaction occurs when SF reacts with calcium hydroxide, which forms additional C-S-H gel, further refining the pore structure [54].

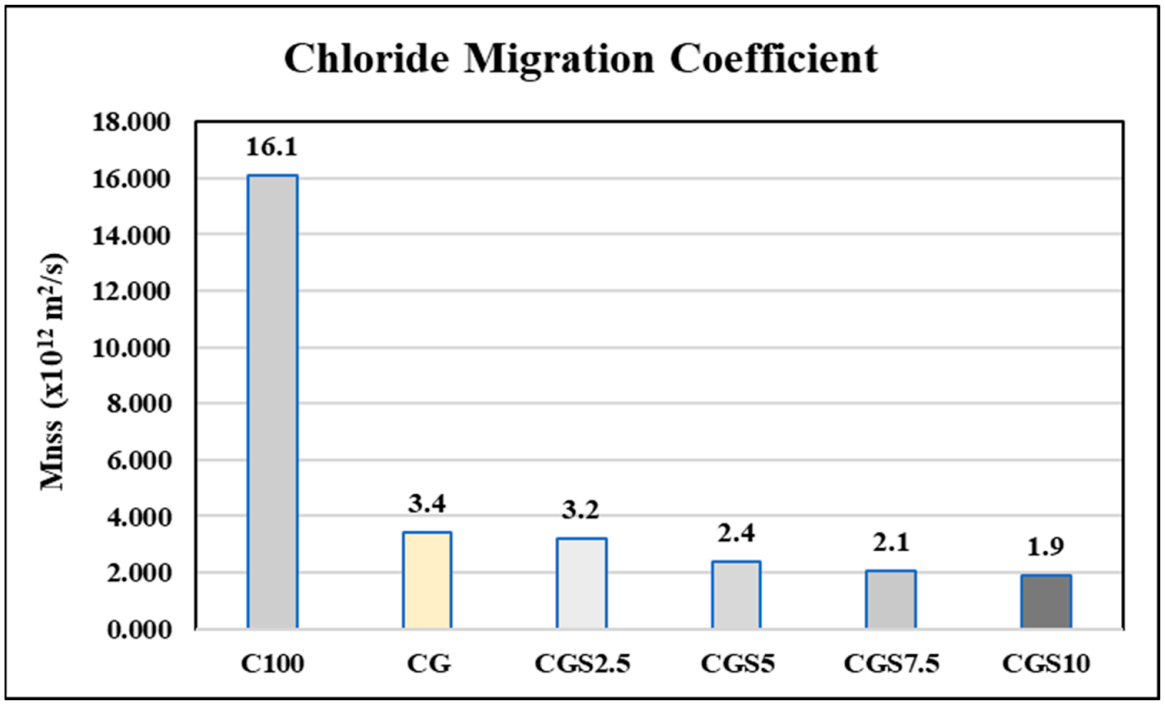


Figure 17. Chloride migration coefficient of each mix.

3.5. Accelerated Carbonation Penetration

Figures 18 and 19 illustrate the carbonation depth of each mix after 7 and 14 days of carbonation exposure. Phenolphthalein solution was sprayed on the freshly split surface of the samples as a pH indicator, which indicates pH values above 8. In non-carbonated areas, the phenolphthalein reacts with calcium hydroxide, turning the concrete purple. Carbonation takes place when carbon dioxide reacts with calcium hydroxide, resulting in the formation of calcium carbonate. Since calcium carbonate has a pH lower than 8, it does not cause a colour change with phenolphthalein. The carbonation depth was measured by identifying the non-purple zone as the carbonated region [55].

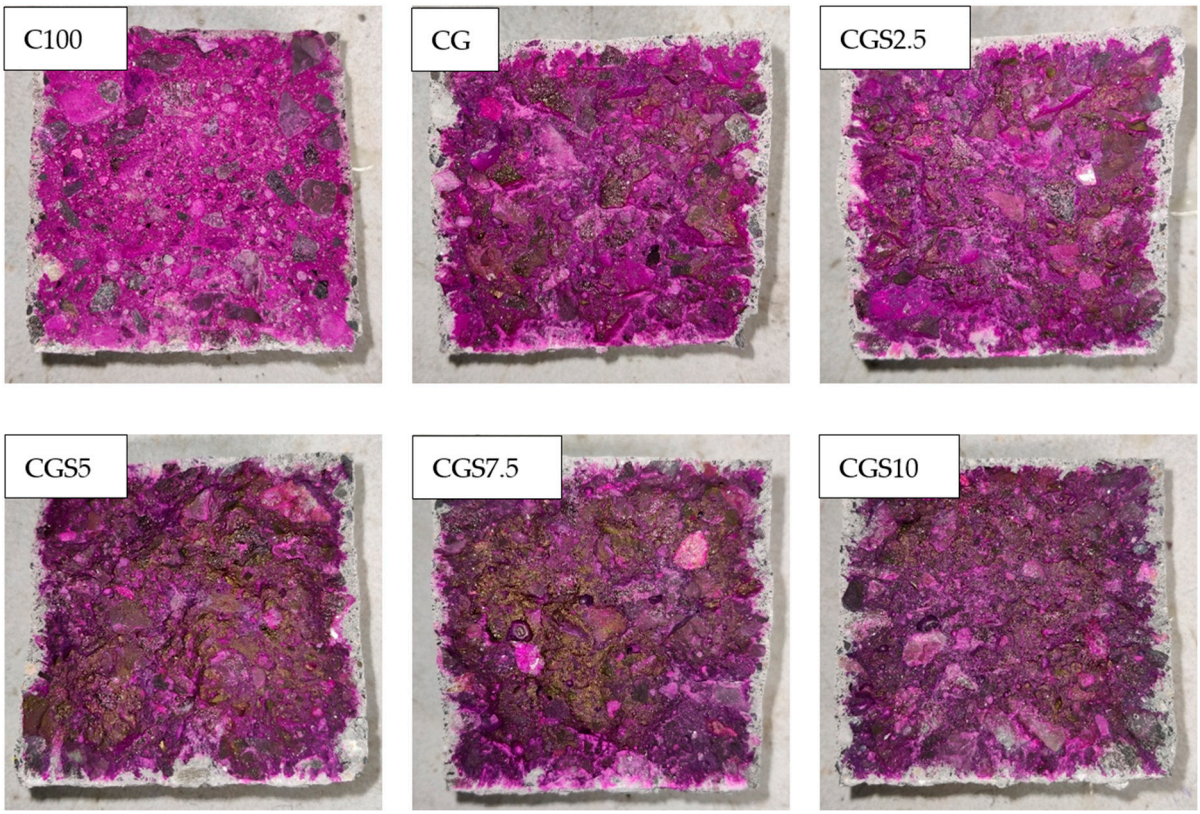


Figure 18. Seven-day carbonation exposure penetration depth.

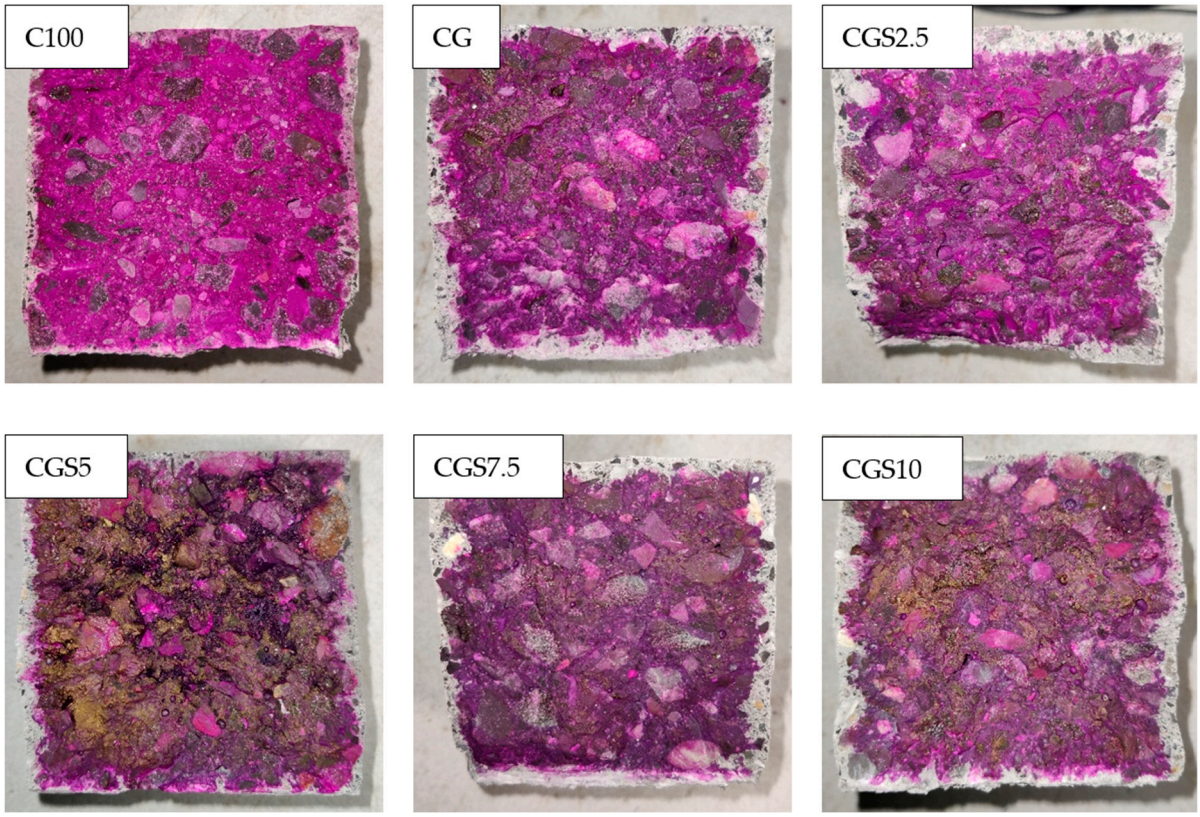


Figure 19. Fourteen-day carbonation exposure penetration depth.

Figure 20 depicts the graph drawn for the carbonation depth and square root of time in days to determine the K_{AC} value of the concrete mixes, and Figure 21 compares the

different carbonation depths after 7-day, 14-day and 28-day exposure. After 7 days, 14 days, and 28 days, C100 had the least carbonation depth at 2.89 mm, 3.01 mm, and 3.82 mm, respectively. The carbonation depth increased by 25.4% to 3.62 mm at 7 days, by 48.5% to 4.47 mm at 14 days, and by 6.3% to 4.06 mm at 28 days with the addition of GGBS in CG. Zhao et al. found a similar increase in carbonation depth with the replacement of 50% GGBS [56]. This is caused by the consumption of calcium hydroxide by the GGBS during the formation of C-S-H gels [56]. The calcium hydroxide or portlandite gives the concrete the ability to resist carbonation. Moreover, GGBS causes delayed hydration, which leads to inadequate curing, and a porous microstructure decreases the carbonation resistance [57]. The addition of SF in CGS2.5 and CGS5 causes the carbonation depth to increase further to 3.89 mm and 3.87 mm, respectively, at 7 days. SF is highly reactive and reacts with calcium hydroxide to create C-S-H gels, decreasing the ability to resist carbonation. At 28 days, all mixes containing SF showed greater carbonation depth compared to the control mix (C100). However, the carbonation depth gradually decreased as the SF dosage increased, likely due to pore refinement that decreases concrete permeability, reaching its lowest at 7.5% replacement but still greater than C100. Since cement is the primary source of calcium hydroxide, its replacement with GGBS and SF lowers initial alkalinity, and their subsequent reactions further deplete the available calcium hydroxide, significantly compromising carbonation resistance.

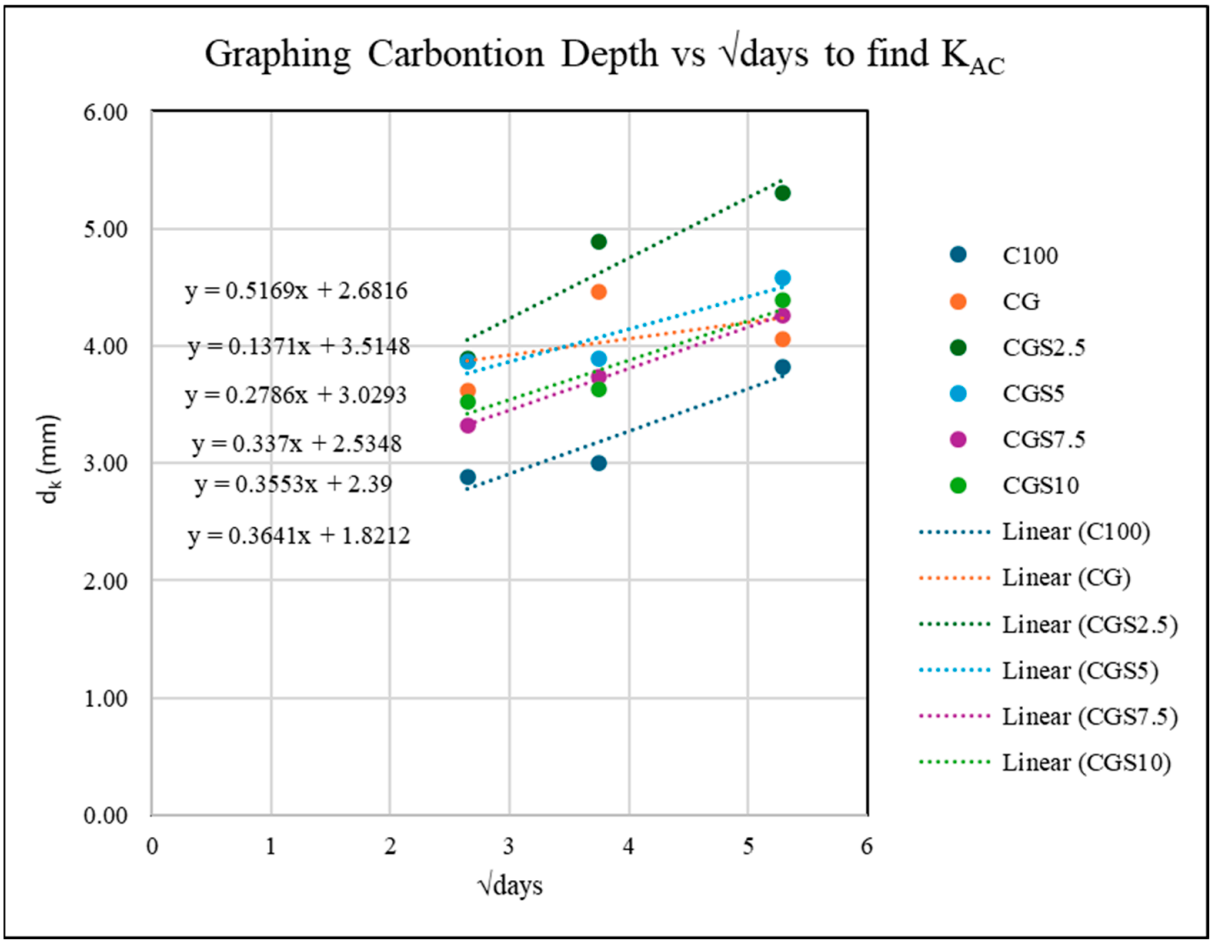


Figure 20. Determination of the carbonation coefficient (K_{AC}) of concrete mixes.

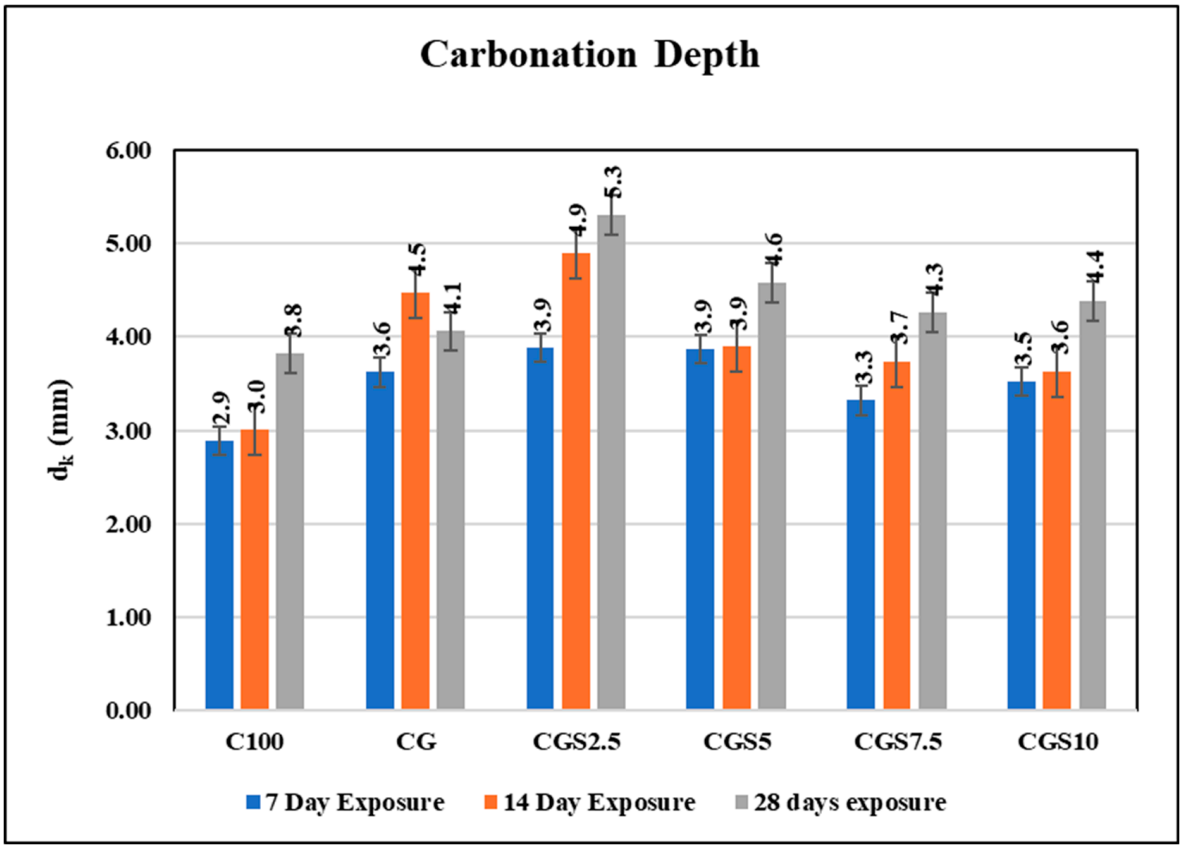


Figure 21. Carbonation penetration for each mix.

4. Discussion

4.1. Printability

A concrete mix must be considered to have a high level of printability to make it usable as 3DPC. The two primary factors influencing printability are pumpability and buildability [58]. Pumpability is the ability for concrete to be pumped to the printer head, and buildability is focused on shape retention and early-age strength to support subsequent layers, as well as ensuring adequate interlayer bonding. Tay et al. [59] evaluated the printability of concrete based on criteria that relate slump and slump flow tests to key performance aspects. The slump test is more indicative of shape retention [59]. However, the determination of the interlayer bond strength through direct tensile testing and shear bond testing is necessary to perfectly analyze the interlayers of 3D-printed elements in the future. Slump test results indicate that CGS7.5 and CGS10 exhibit slump values of 21 cm and 19.5 cm, respectively. As shown in Figure 10, these mixes can also retain their shape, similar to C100. The CGS5 mix shows moderate shape retention with a slump of 23.5 cm, while CGS2.5 and CG display no shape retention. However, both CGS2.5 and CG demonstrate high flowability, suggesting their suitability for pumping, but this needs to be verified in future through rheology. CGS5 demonstrates a high flowability with better consistency, making it ideal for pumping. Similarly, the printability of CG, CGS7.5, and CGS10 appears promising due to their similarity in cohesiveness to CGS5. These observations highlight that incorporating SF into low-carbon concrete mixes enhances the printability of 3DPC. This causes an improvement in the interlayer bond, which increases the durability of the concrete. To further strengthen this evaluation, more quantitative criteria for pumpability and buildability (such as rheological measurements to obtain yield stress and plastic viscosity and buildability derived from layer deformation or height retention tests) need to be evaluated in future.

4.2. Mechanical Properties

The most significant mechanical property of 3DPC is the compressive strength. From the compressive strength results, it was found that replacing cement with GGBS by 50% reduces the 1-day compressive strength by 58.5%. Although the strength of the fresh concrete was not investigated, the reduced strength at 1 day suggests that all the low-carbon mixes used are still suitable for 3DPC, as they meet the minimum early strength requirements for structural buildability and can support subsequent layers during the printing process, but need to be assessed in future. This highlights the adequacy of low-carbon concrete as a blockwork replacement, without even considering the significant long-term strength gain observed at 7 and 28 days. However, to fully assess its mechanical suitability, the fresh-state mechanical performance of the low-carbon mix must be further investigated.

4.3. Durability Enhancements

As previously highlighted, the interlayer interface in 3DPC represents a critical zone of weakness, as the material does not behave as a fully homogeneous solid. This discontinuity can lead to the formation of voids and microcracks, which facilitate the ingress of air and liquids, thereby compromising durability. Furthermore, the incorporation of additives such as GGBS and SF, as demonstrated in this study, can significantly enhance resistance to chemical attacks.

4.3.1. Chloride Resistance

It was evident from the results that the incorporation of GGBS significantly enhances the concrete's resistance to chloride penetration, as illustrated in Figure 17. The CG mix containing 50% GGBS exhibited 4.7 times greater resistance compared to the C100 mix, which used 100% cement as the binder. This improvement is attributed to the formation of a denser microstructure and the generation of Friedel's salts, which reduce chloride permeability in the concrete [60]. Additionally, the inclusion of SF further improved the chloride resistance of the concrete mixes. An increase in SF dosage from 2.5% to 10% led to a corresponding increase in chloride resistance. This enhancement is likely due to the additional refinement of the microstructure through the formation of calcium silicate hydrate (C-S-H) gels during the pozzolanic reaction.

4.3.2. Carbonation Resistance

The carbonation exposure results, as shown in Figure 21, indicate that the incorporation of GGBS and SF adversely affects the carbonation resistance of concrete at early ages. Specifically, the inclusion of GGBS reduced the carbonation resistance by more than 1.06 times at 28 days compared to the control mix. This is attributed to the consumption of calcium hydroxide in the formation of C-S-H gels, which leads to a scarcity of calcium hydroxide to react with the penetrated carbon dioxide to form calcium carbonate and slows down the carbonation process [61]. Although SF addition reduces carbonation resistance, this is an important factor for 3D-printed elements, as interlayer zones are more prone to CO_2 penetration and localized carbonation. This effect can be significant in aggressive outdoor or reinforced applications but minimal in interior or non-reinforced components. Mitigation measures such as surface treatments or interlayer densification can minimize carbonation risk and enhance long-term durability [19]. However, it is worth noting that during over-extended curing periods, the continued development of a denser microstructure that will be facilitated by GGBS and SF may eventually enhance carbonation resistance by limiting carbon dioxide ingress [62]. The higher CaO content in GGBS promoted additional C-S-H and C-A-S-H gel formation, refining pores and enhancing strength and chloride resistance. However, increased SF reduced overall calcium availability, lowering

the C/S ratio and producing a more silica-rich gel with less buffering capacity against CO_2. As a result, carbonation depth followed a non-linear trend, and moderate SF improved microstructure and strength, while excessive replacement increased carbonation due to reduced calcium content [10]. Further long-term studies in future are needed to confirm this potential improvement. To limit the increased carbonation observed at higher SF contents, approaches such as optimizing SCM replacement levels and incorporating small doses of reactive nano-additives can be effective. Prolonged moist curing further reduces CO_2 ingress. Also, it is recommended to take pore-refinement measures with targeted chemistry control by maintaining an adequate amount of Ca $(OH)_2$ when developing low-carbon mixes [63].

4.4. Sustainability Trade-Off

3DPC holds significant potential for enhancing sustainability in the construction industry. One of its key advantages is the precision it offers in material usage, and accurate digital modelling enables concrete to be placed exactly where it is needed, reducing overproduction and minimizing onsite waste. This efficiency not only reduces raw material consumption but also lowers energy demands related to transport and formwork fabrication, as 3DPC eliminates the need for traditional moulds. The environmental benefits can be further amplified by incorporating low-carbon concrete mixes. In this study, GGBS was used as a 50% replacement for cement, resulting in a 44% reduction in carbon emissions. The inclusion of SF contributed to additional emission savings. This aligns with global efforts to decarbonize the construction sector and transition toward a circular economy. A suitable trade-off between concrete performance and carbon emission reduction is essential to ensure its viability as an alternative [64].

To quantify the sustainability trade-off more clearly, the optimum mix (CGS5) demonstrated a 45.5% reduction in carbon footprint compared to the control mix (C100). However, the sustainability of 3DPC must be balanced against performance requirements. While the early-age strength of the low-carbon mix is lower, it remains adequate for targeted 3D printing applications, particularly in non-structural or prefabricated blocks. For larger-scale or load-bearing structures, further mix optimization may be required. While the 5% SF mix significantly reduced embodied carbon, its slightly higher carbonation depth may affect the durability of 3D-printed elements in CO_2-rich environments. The aim is to minimize carbonation susceptibility through optimized mix design, curing, and protective measures to ensure sustainable long-term performance, as reported in previous research [65]. Ultimately, with continued innovation and validation, 3DPC combined with sustainable binders can play a transformative role in achieving greener construction.

5. Conclusions and Future Recommendations

This study investigates the impact of silica fume on the fresh, mechanical, and selected durability properties of low-carbon 3DPC. Based on the results from testing, the following conclusions can be made.

- The incorporation of GGBS and SF improved the overall durability, increasing chloride resistance by up to 4.7 times compared to the control mix.
- Slump test results show that adding GGBS increased the measured slump by 1.2 times, while the addition of SF caused a linear decrease in slump, indicating improved mix cohesiveness. A 5% SF content provided the most suitable workability for 3D printing applications.
- GGBS reduced early compressive strength by 58.5%, and adding 7.5% SF further decreased strength by 12.7% at 7 days. However, at 28 days, the low-carbon mix (CG)

and the 5% SF mix (CGS5) achieved 4.2% and 6% higher strength, respectively, than the control.

- Low-carbon mixes containing GGBS showed 25.4% higher carbonation depth, and SF addition increased carbonation up to 7.5% content, after which the rate stabilized.
- Replacing cement with GGBS and SF substantially reduced carbon emissions, producing a more sustainable mix. The suitability of the mixes for the potential application of 3D printing was assessed based on their slump, strength, and selected durability performance.
- While SF slightly reduced early-age strength and carbonation resistance, these effects were offset by a 6% gain in 28-day strength and a 6.7-fold improvement in chloride resistance compared to C100.
- Overall, a 5% SF replacement achieved the best balance of workability, strength, and durability for low-carbon 3D-printable concrete.

Future work will employ standard 3D printing tests, including buildability, rheological characterization, interlayer bond, and open time measurements to optimize the balance between pumpability and shape retention, as reported in a previous study [66]. Also, there is a need for future work to confirm the early-age carbonation behavior observed with GGBS/SF mixes under natural field conditions and thermal behavior at elevated temperatures. Additionally, future work should focus on comprehensive microstructural characterization using MIP, SEM-EDS, and XRD to provide direct evidence of chloride binding, pore refinement, and phase evolution (e.g., Friedel's salt formation) underlying the observed durability performance.

Author Contributions: J.B.: conceptualization, validation, formal analysis, methodology, investigation, data curation, writing—original draft preparation; S.B.: writing—review and editing, visualization, software, validation, formal analysis, data curation; W.S.: Writing—review and editing, visualization, software, methodology, investigation, formal analysis, data curation; M.K.: project administration, writing—review and editing, methodology, investigation, formal analysis, supervision, conceptualization, funding acquisition; C.M.: writing—review and editing, visualization, methodology, funding acquisition, project administration, conceptualization, supervision. All authors have read and agreed to the published version of the manuscript.

Funding: This publication emanated from two separate projects. The first is funded by Construct Innovate Technology Centre and Harcourt Technologies Limited (HTL) (Grant Code: CISFC1-24_018). The second is funded by Ecocem Materials and the Science Foundation Ireland (SFI) Research Centre in Applied Geosciences hosted by UCD (iCRAG-Phase 2-Grant Code: 13/RC/2092_P2).

Data Availability Statement: The original contributions presented in this study are included in the article. Further inquiries can be directed to the corresponding authors.

Acknowledgments: The authors gratefully acknowledge Ecocem Materials Ireland for providing GGBS, Irish Cement for supplying CEM II/A-L 42.5N, Roadstone for providing aggregates, and Sika Ireland Ltd. for supplying the superplasticizer, silica fume, and Sika fibres.

Conflicts of Interest: The authors declare no conflicts of interest.

References

1. Kanagaraj, B.; Priyanka, R.; Anand, N.; Kiran, T.; Andrushia, A.D.; Lubloy, E. A sustainable solution for mitigating environmental corrosion in the construction sector and its socio-economic concern. *Case Stud. Constr. Mater.* **2024**, *20*, e03089. [CrossRef]
2. Craveiro, F.; Nazarian, S.; Bartolo, H.; Bartolo, P.J.; Pinto Duarte, J. An automated system for 3D printing functionally graded concrete-based materials. *Addit. Manuf.* **2020**, *33*, 101146. [CrossRef]
3. Hanratty, N.; Khan, M.; McNally, C. The Role of Different Clay Types in Achieving Low-Carbon 3D Printed Concretes. *Buildings* **2024**, *14*, 2194. [CrossRef]

4. Zhang, J.; Wang, J.; Dong, S.; Yu, X.; Han, B. A review of the current progress and application of 3D printed concrete. *Compos. Part A Appl. Sci. Manuf.* **2019**, *125*, 105533. [CrossRef]
5. Nodehi, M.; Aguayo, F.; Nodehi, S.E.; Gholampour, A.; Ozbakkaloglu, T.; Gencel, O. Durability properties of 3D printed concrete (3DPC). *Autom. Constr.* **2022**, *142*, 104479. [CrossRef]
6. Firoozi, A.; Firoozi, A.; Oyejobi, D.O.; Avudaiappan, S.; Flores, E. Enhanced durability and environmental sustainability in marine infrastructure: Innovations in anti-corrosive coating technologies. *Results Eng.* **2025**, *26*, 105144. [CrossRef]
7. Khan, M.; McNally, C. Recent developments on low carbon 3D printing concrete: Revolutionizing construction through innovative technology. *Clean. Mater.* **2024**, *12*, 100251. [CrossRef]
8. Zhang, Y.; Zhang, Y.; She, W.; Yang, L.; Liu, G.; Yang, Y. Rheological and harden properties of the high-thixotropy 3D printing concrete. *Constr. Build. Mater.* **2019**, *201*, 278–285. [CrossRef]
9. Swathi, B.; Vidjeapriya, R. Influence of precursor materials and molar ratios on normal, high, and ultra-high performance geopolymer concrete—A state of art review. *Constr. Build. Mater.* **2023**, *392*, 132006. [CrossRef]
10. Swathi, B.; Vidjeapriya, R. Synergistic use of nano-silica to enhance the characterization of ambient-cured geopolymer concrete. *Arch. Civ. Mech. Eng.* **2023**, *24*, 4. [CrossRef]
11. Bukhari, S.J.S.; Khanzadeh Moradllo, M. Multicriteria performance assessment of 'low w/c + low cement + high dosage admixture' Concrete: Environmental, economic, durability, and mechanical performance considerations. *J. Clean. Prod.* **2025**, *523*, 146419. [CrossRef]
12. Bouchelil, L.; Shah Bukhari, S.J.; Khanzadeh Moradllo, M. Evaluating the performance of internally cured limestone calcined clay concrete mixtures. *J. Sustain. Cem.-Based Mater.* **2024**, *14*, 198–208. [CrossRef]
13. Swathi, B.; Vidjeapriya, R. Stimulation of calcium (Sodium)-alumina-silicate-hydrate (C(N)-A-S-H) gel by nano-alumina in the cleaner production of agro-based alkali-activated concrete. *Sustain. Chem. Pharm.* **2025**, *46*, 102100. [CrossRef]
14. Fahim, A.A.; Bukhari, S.J.S.; Khanzadeh Moradllo, M. Additive manufacturing of carbonatable ternary cementitious systems with cellulose nanocrystals. *Constr. Build. Mater.* **2025**, *495*, 143753. [CrossRef]
15. Singh, A.; Anand, K.; Liu, Q.; Tam, V.Y.; Goyal, S.; Reddy, M.S. Enhancing interlayer bonding in 3-dimensional printed concrete using bacteria-based biomineralization. *Cem. Concr. Compos.* **2025**, *164*, 106258. [CrossRef]
16. Si, W.; Hopkins, B.; Khan, M.; McNally, C. Towards Sustainable Mortar: Optimising Sika-Fibre Dosage in Ground Granulated Blast Furnace Slag (GGBS) and Silica Fume Blends for 3D Concrete Printing. *Buildings* **2025**, *15*, 3436. [CrossRef]
17. Si, W.; Carr, L.; Zia, A.; Khan, M.; McNally, C. Advancing 3D Printable Concrete with Nanoclays: Rheological and Mechanical Insights for Construction Applications. *J. Compos. Sci.* **2025**, *9*, 449. [CrossRef]
18. Si, W.; Khan, M.; McNally, C. Effect of nano silica with high replacement of GGBS on enhancing mechanical properties and rheology of 3D printed concrete. *Results Eng.* **2025**, *27*, 106680. [CrossRef]
19. Bradshaw, J.; Si, W.; Khan, M.; McNally, C. Emerging Insights into the Durability of 3D-Printed Concrete: Recent Advances in Mix Design Parameters and Testing. *Designs* **2025**, *9*, 85. [CrossRef]
20. Zhou, L.; Gou, M.; Ji, J.; Hou, X.; Zhang, H. Durability and hardened properties of 3D printed concrete containing bauxite tailings. *Mater. Today Sustain.* **2024**, *25*, 100704. [CrossRef]
21. Si, W.; Khan, M.; McNally, C. A Comprehensive Review of Rheological Dynamics and Process Parameters in 3D Concrete Printing. *J. Compos. Sci.* **2025**, *9*, 299. [CrossRef]
22. Hopkins, B.; Si, W.; Khan, M.; McNally, C. Recent Advancements in Polypropylene Fibre-Reinforced 3D-Printed Concrete: Insights into Mix Ratios, Testing Procedures, and Material Behaviour. *J. Compos. Sci.* **2025**, *9*, 292. [CrossRef]
23. Firoozi, A.A.; Firoozi, A.A.; Oyejobi, D.O.; Avudaiappan, S.; Flores, E.S. Emerging trends in sustainable building materials: Technological innovations, enhanced performance, and future directions. *Results Eng.* **2024**, *24*, 103521. [CrossRef]
24. Waite, R. How a Social Housing Scheme Pioneered 3D Printing. 2025. Available online: https://www.architectsjournal.co.uk/news/how-a-social-housing-scheme-pioneered-3d-printing (accessed on 24 January 2025).
25. Doris. 3D Concrete Printing Market to Reach $56.4 Million by 2021. 2016. Available online: https://www.3printr.com/3d-concrete-printing-market-reach-56-4-million-2021-1239664/ (accessed on 2 June 2016).
26. Roadstone. First Viewing of Ireland's 3D Printed Social Housing. 2024. Available online: https://www.roadstone.ie/news/first-viewing-irelands-3d-printed-social-housing (accessed on 16 December 2024).
27. El-Sayegh, S.; Romdhane, L.; Manjikian, S. A critical review of 3D printing in construction: Benefits, challenges, and risks. *Arch. Civ. Mech. Eng.* **2020**, *20*, 34. [CrossRef]
28. Jia, L.; Niu, G.; Dong, E.; Jiang, Y.; Wang, X.; Jia, Z.; Wang, W.; Gao, Y.; Zhang, Y. Optimization strategy for incorporating recycled brick powder in 3D-printed concrete by balancing low carbon footprint and enhanced performance. *Constr. Build. Mater.* **2024**, *443*, 137801. [CrossRef]
29. De Bono, V.; Ducoulombier, N.; Mesnil, R.; Caron, J.F. Methodology for formulating low-carbon printable mortar through particles packing optimization. *Cem. Concr. Res.* **2024**, *176*, 107403. [CrossRef]

30. Jin, P.; Hasany, M.; Kohestanian, M.; Mehrali, M. Micro/nano additives in 3D printing concrete. *Cem. Concr. Compos.* **2025**, *155*, 105799. [CrossRef]
31. Zhao, R.; Jin, Z.; Feng, G.; Li, J.; Liu, J. Chloride Diffusion and Induced Reinforcement Corrosion in Concrete with Fly Ash and Ground-Granulated Blast-Furnace Slag Exposed to Marine Submerged Zone. *Adv. Mater. Sci. Eng.* **2020**, *2020*, 8881446. [CrossRef]
32. Huang, X.; Yang, W.; Song, F.; Zou, J. Study on the mechanical properties of 3D printing concrete layers and the mechanism of influence of printing parameters. *Constr. Build. Mater.* **2022**, *335*, 127496. [CrossRef]
33. Zhao, Y.; Gao, Y.; Chen, G.; Li, S.; Singh, A.; Luo, X.; Liu, C.; Gao, J.; Du, H. Development of low-carbon materials from GGBS and clay brick powder for 3D concrete printing. *Constr. Build. Mater.* **2023**, *383*, 131232. [CrossRef]
34. Cui, W.; Shen, L.; Ji, D.; Liu, W.; Wang, T.; Hou, D.; Shen, W.; Shi, X.; Tao, Y. Mechanical performance and permeability of low-carbon printable concrete. *J. Sustain. Cem.-Based Mater.* **2024**, *14*, 406–416. [CrossRef]
35. *I.S. EN 197-1*; Cement—Part 1: Composition, Specifications and Conformity Criteria for Common Cements. NSAI—National Standards Authority of Ireland, (CEN): Dublin, Ireland, 2011.
36. *I.S. EN 15167-1*; Ground Granulated Blast Furnace Slag for Use in Concrete, Mortar and Grout—Part 1: Definitions, Specifications and Conformity Criteria. NSAI—National Standards Authority of Ireland, (CEN): Dublin, Ireland, 2006.
37. *I.S. EN 13263-2*; Silica Fume for Concrete—Part 2: Conformity Evaluation. NSAI—National Standards Authority of Ireland, (CEN): Dublin, Ireland, 2009.
38. Sika. *Viscocrete-10 Product Data Sheet*; Sika: Baar, Switzerland, 2019.
39. Zhu, X.; Zhang, Y.; Liu, Z.; Qiao, H.; Ye, F.; Lei, Z. Research on carbon emission reduction of manufactured sand concrete based on compressive strength. *Constr. Build. Mater.* **2023**, *403*, 133101. [CrossRef]
40. Cement, I. *Environmental Production Declaration CEM II*; The European Cement Association: Brussels, Belgium, 2022.
41. Ecocem. *GGBS Technical Data Sheet*; Ecocem: Dublin, Ireland, 2023.
42. Elkem. *Benefits of Elkem Microsilica in Concrete*; Elkem: Cliffwood, NJ, USA, 2017.
43. Roadstone. *Roadstone Aggregates & Granular—EDP*; Roadstone: Stoughton, MA, USA, 2023.
44. Sika. *ViscoCrete-2100 Environmental Production Declaration*; Sika: Baar, Switzerland, 2023.
45. *EN 12390-2*; Testing hardened concrete—Part 2: Making and Curing Specimens for Strength Tests. European Standard: Brussels, Belgium, 2019.
46. *ISO 1920-2:2016*; Testing of Concrete—Part 2: Properties of Fresh Concrete. ISO: Geneva, Switzerland, 2016.
47. *EN12390-3-2019*; Testing Hardened Concrete—Part 3: Compressive Strength of Test Specimens. European Standard: Brussels, Belgium, 2019.
48. *EN 12390-18:2021+A1:2024*; Testing Hardened Concrete—Part 18: Determination of the Chloride Migration Coefficient. European Standard: Brussels, Belgium, 2021.
49. Bernal, S.A.; Dhandapani, Y.; Elakneswaran, Y.; Gluth, G.J.G.; Gruyaert, E.; Juenger, M.C.G.; Lothenbach, B.; Olonade, K.A.; Sakoparnig, M.; Shi, Z.; et al. Report of RILEM TC 281-CCC: A critical review of the standardised testing methods to determine carbonation resistance of concrete. *Mater. Struct.* **2024**, *57*, 173. [CrossRef]
50. *EN 12390-12-2020*; Testing Hardened Concrete—Part 12: Determination of the Carbonation Resistance of Concrete—Accelerated Carbonation Method. European Standard: Brussels, Belgium, 2020.
51. Chen, W.; Wu, M.; Liang, Y. Effect of SF and GGBS on Pore Structure and Transport Properties of Concrete. *Materials* **2024**, *17*, 1365. [CrossRef]
52. Mao, Y.; Jiao, D.; Hu, X.; Jiang, Z.; Shi, C. Effect of dispersion behavior of silica fume on the rheological properties and early hydration characteristics of ultra-high strength mortar. *Cem. Concr. Compos.* **2024**, *152*, 105654. [CrossRef]
53. Sun, H.-Q.; Zeng, J.-J.; Hong, G.-Y.; Zhuge, Y.; Liu, Y.; Zhang, Y. 3D-printed functionally graded concrete plates: Concept and bending behavior. *Eng. Struct.* **2025**, *327*, 119551. [CrossRef]
54. Badalyan, M.M.; Muradyan, N.G.; Shainova, R.S.; Arzumanyan, A.A.; Kalantaryan, M.A.; Sukiasyan, R.R.; Yeranosyan, M.; Laroze, D.; Vardanyan, Y.V.; Barseghyan, M.G. Effect of Silica Fume Concentration and Water–Cement Ratio on the Compressive Strength of Cement-Based Mortars. *Buildings* **2024**, *14*, 757. [CrossRef]
55. Ashraf, W. Carbonation of cement-based materials: Challenges and opportunities. *Constr. Build. Mater.* **2016**, *120*, 558–570. [CrossRef]
56. Zhao, J.; Shumuye, E.D.; Wang, Z.; Bezabih, G.A.; Yi, H. Performance of GGBS Cement Concrete under Natural Carbonation and Accelerated Carbonation Exposure. *J. Eng.* **2021**, *2021*, 6659768. [CrossRef]
57. Ahmad, S.; Baghabra Al-Amoudi, O.S.; Khan, S.M.S.; Maslehuddin, M. Effect of silica fume inclusion on the strength, shrinkage and durability characteristics of natural pozzolan-based cement concrete. *Case Stud. Constr. Mater.* **2022**, *17*, e01255. [CrossRef]
58. Fasihi, A.; Libre, N.A. From pumping to deposition: A Comprehensive review of test methods for characterizing concrete printability. *Constr. Build. Mater.* **2024**, *414*, 134968. [CrossRef]
59. Tay, Y.W.D.; Qian, Y.; Tan, M.J. Printability region for 3D concrete printing using slump and slump flow test. *Compos. Part B Eng.* **2019**, *174*, 106968. [CrossRef]

60. Amin, M.T.E.; Sarker, P.K.; Shaikh, F.U.A.; Hosan, A. Chloride permeability and chloride-induced corrosion of concrete containing lithium slag as a supplementary cementitious material. *Constr. Build. Mater.* **2025**, *471*, 140629. [CrossRef]
61. Xian, X.; Shao, Y. Microstructure of cement paste subject to ambient pressure carbonation curing. *Constr. Build. Mater.* **2021**, *296*, 123652. [CrossRef]
62. Zong, Z.; Zhang, Q.; Liu, Y.; Guo, Z.; Lin, S.; Jiang, T. Carbonation resistance of sustainable self-compacting concrete with recycled concrete aggregate and fly ash, slag, and silica fume. *Eur. J. Environ. Civ. Eng.* **2023**, *28*, 2177–2199. [CrossRef]
63. Sun, H.-Q.; Zeng, J.-J.; Xie, S.-S.; Xia, J.-R.; Yu, S.; Zhuge, Y. Mechanical and microstructural characterization of interlayer bonding in multi-material 3D-Printed concrete. *Cem. Concr. Compos.* **2026**, *165*, 106308. [CrossRef]
64. Al Khaffaf, I.; Hawileh, R.A.; Sahoo, S.; Abdalla, J.A.; Kim, J.H. Toward carbon- neutral construction: A review of zero-carbon concrete. *J. Build. Eng.* **2025**, *99*, 111578. [CrossRef]
65. Ramadan, S.; Kassem, H.; Elkordi, A.; Joumblat, R. Advancing Pavement Sustainability: Assessing Recycled Aggregates as Substitutes in Hot Mix Asphalt. *Sustainability* **2025**, *17*, 5472. [CrossRef]
66. Zeng, J.-J.; Sun, H.-Q.; Deng, R.-B.; Yan, Z.-T.; Zhuge, Y. Bond performance between FRP bars and 3D-printed high-performance concrete. *Structures* **2025**, *73*, 108377. [CrossRef]

Disclaimer/Publisher's Note: The statements, opinions and data contained in all publications are solely those of the individual author(s) and contributor(s) and not of MDPI and/or the editor(s). MDPI and/or the editor(s) disclaim responsibility for any injury to people or property resulting from any ideas, methods, instructions or products referred to in the content.